Colloid Polym Sci 277:1193–1199 (1999)

ORIGINAL CONTRIBUTION

P. Müller-Buschbaum
J.S. Gutmann
R. Cubitt
M. Stamm

Probing the in-plane composition of thin polymer films with grazing-incidence small-angle neutron scattering and atomic force microscopy

Received: 13 April 1999
Accepted in revised form: 29 June 1999

P. Müller-Buschbaum (✉)[1]
J.S. Gutmann · M. Stamm
MPI für Polymerforschung
Ackermannweg 10
D-55128 Mainz, Germany

R. Cubitt
ILL, Avenue des Martyrs, B.P. 156
F-38042 Grenoble, France

[1] *Present address*:
TU München, Physik Department, LS E13,
James-Franck-Strasse 1
D-85747 Garching, Germany

Abstract The surface morphologies of confined, dewetted polymer films were investigated with atomic force microscopy (AFM) and grazing-incidence small-angle neutron scattering (GISANS). On examining homopolymer films of deuterated polystyrene (dPS) both techniques reveal the resulting droplet structure which is described by one most prominent in-plane length. Due to the contrast resulting from deuteration in the case of polymer blend films of dPS and poly(*p*-methyl styrene) GISANS is able to probe the in-plane composition of the dewetting structure. An additional phase separation process at different length scales gives rise to a sub- and superstructure which is not detectable by AFM. In addition, the influence of the wavelength used in the GISANS experiments on the structures observed is discussed.

Key words Neutron scattering · Polymer blend · Thin films

Introduction

A number of practical applications such as coatings, paints, printings or biomaterials are controlled or limited by the dewetting of an originally homogeneous thin film on top of a solid. The dewetting of homopolymer films on nonwettable surfaces has been intensively investigated [1–10]. Many practical applications, however, do not use homopolymers but use polymer blends. In polymer blend thin film systems the phase separation behavior has mainly been investigated [11–17]. Less attention has been paid to the interplay between phase separation and dewetting of thin polymer blend films on top of nonwettable surfaces [18, 19]. All investigations concerning polymer blend films can be divided into three regimes with respect to the prepared film thickness. For thick polymer blend films due to the existence of two boundary interfaces and generally a preferential segregation of one or the other component of the blend to the interfaces, the development of composition waves normal to the surface is induced. This surface-directed spinodal decomposition can propagate some wavelengths into the film before decaying into an isotropic bicontinuous spinodal bulk pattern. In thin blend films with film thicknesses below a critical thickness these composition waves normal to the surface are suppressed [20]. On reducing the film thickness further to values below the radius of gyration (R_g) of the unperturbed molecule the third regime is entered. These extremely thin films represent an additional range of polymeric material, which is characterized by the special conformation of the polymer chains [21]. The confinement yields changes in the thermodynamical behavior [22–25] and, depending on the substrate interaction dewetting can occur. Due to the thin film thickness these films can be regarded as two-dimensional. For the molecular weight of the investigated samples R_g is of the order of 10 nm; therefore, confined polymer blend films have an extremely small scattering volume. In addition, they have to be prepared on top of solid substrates to investigate the interplay between dewetting and phase separation. Both factors make a common transmission

geometry disadvantageous. Even the use of a sample stack consisting of several similarly prepared samples only gives rise to a scattering signal which contains a small contribution of the polymer film. One way to overcome this problem is the use of a reflection geometry as demonstrated previously with X-ray scattering techniques [26]: it extends the largest resolvable length scale with respect to a transmission set-up [27]. However, in the case of X-rays, contrast even for significantly different polymers is not large, whereas with neutrons strong contrast between two components can be generated by deuteration. This is extremely useful for investigations on blends of weakly incompatible polymers and has been successfully applied in specular neutron scattering. Specular neutron scattering is a well-established technique for investigating the density profile perpendicular to the sample surface [28–30]. In contrast to diffuse X-ray scattering [31–33] the use of off-specular neutron scattering for probing the lateral morphology of surfaces and interfaces is only rarely applied [34–36]. Experiments utilizing grazing-incidence small-angle neutron scattering (GISANS) are not reported in the literature. This may result from the limited intensities available with neutrons compared to X-rays.

Experimental

Neutron scattering

The GISANS experiments were performed at the D22 beamline at the ILL (Grenoble). We operated the instrument in the wavelength regime of the highest available neutron flux with respect to the necessary resolution as discussed later. Thus we used wavelengths of 0.7, 1.0 and 1.4 nm (wavelength selector; $\Delta\lambda/\lambda = 10\%$). Details concerning the beamline are reported elsewhere [37]. We applied a reflection geometry with a vertically mounted sample instead of the commonly used transmission geometry. The beam divergence in and out of the plane of reflection was limited by two entrance cross slits. The nonspecular as well as the specular intensity was recorded with a two-dimensional detector consisting of a 128×128 pixel array. A schematic drawing of the experimental set-up is shown in Fig. 1. The primary beam is shielded with a beam stop. The incident angle is denoted by α_i, the exit angle by α_f and the out-of-plane angle by ψ. With a sample–detector distance of 17.66 m and a wavelength of 1.4 nm we achieve a resolution better than $1.91 \times 10^{-3}\,\mathrm{nm}^{-1}$. This enables the detection of in-plane length scales, ξ, of up to 3.3 μm, which is a significant increase compared to the highest resolvable length scale in the transmission geometry under comparable conditions. Nevertheless with the use of even longer wavelengths this value could have been increased further but the decreasing neutron flux would have made the experiments even more difficult. Using a wavelength of 0.7 nm length scales down to 26 nm are detectable. Thus the roughness properties of the samples can be investigated between the molecular and a mesoscopic range.

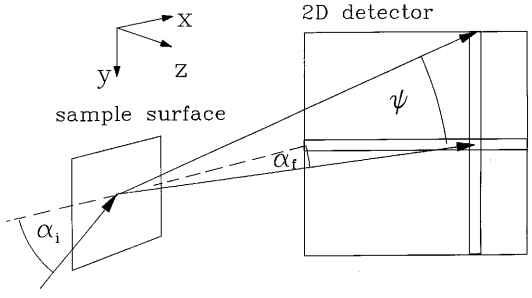

Fig. 1 Experimental set-up of the grazing-incidence small-angle neutron scattering (*GISANS*) experiments at the D22 beamline. The angle of incidence of the neutron beam onto the vertically placed sample surface is denoted by α_i, the exit angle by α_f and the out-of-plane angle by ψ. Specularly as well as diffusely scattered intensity is recorded with the 2D detector

Sample preparation

The confined homogeneous polymer films were prepared on top of native oxide-covered Si(100) surfaces (MEMC Electronic Materials, Spartanburg) by spin-coating (1950 rpm for 30 s) a toluene solution. Prior to spin-coating the silicon substrates were cleaned in a bath of 80% H_2SO_4 (100 ml), H_2O_2 (35 ml) and deionized water (15 ml) for 15 min at 80 °C, rinsed in deionized water and dried with compressed nitrogen. Immediately before coating the dry substrates were flushed with fresh toluene. Deuterated polystyrene (dPS) with a molecular weight $M_w = 157\,\mathrm{kg/mol}$ ($M_w/M_n = 1.09$, $R_g = 10.6\,\mathrm{nm}$) as well as poly(*p*-methyl styrene) (PpMS) with a molecular weight $M_w = 157\,\mathrm{kg/mol}$ ($M_w/M_n = 1.06$, $R_g = 10.0\,\mathrm{nm}$) were used in an asymmetric blend composition of PpMS:dPS = 3:2. Additionally homopolymer samples of dPS were prepared for comparison. The film thickness of the samples was measured by X-ray reflectivity right after preparation. The value of $3.2 \pm 0.2\,\mathrm{nm}$ determined (error bar includes the deviation in the film thickness between different samples) is only one-third of R_g of the unperturbed molecule; thus the polymer molecules are strongly confined. The measured root mean square-surface roughness of $\sigma = 0.3 \pm 0.1\,\mathrm{nm}$ agrees well with the observation of smooth and featureless surfaces in atomic force microscopy (AFM) measurements. The samples were examined as prepared and then annealed under vacuum for 8 h at 161 °C, which is well above the glass-transition temperature. In addition the as-prepared samples were stored 7 for h in a toluene atmosphere. To check the reproducibility of the observed structures several samples were prepared and examined.

Atomic force microscopy

The real space surface topography of the as-prepared as well as of the treated samples was investigated with a PARK Autoprobe CP atomic force microscope in air at room temperature. Several images were measured for each sample. All measurements were performed at different scan ranges in noncontact mode in order to minimize the tip-induced sample degradation. From the surface data of each sample and the scan range the two-dimensional power spectral density (PSD) function was calculated and radially averaged. Combining the data of different scan ranges, with respect to the individual scan size, yields a master curve [38] and thus enlarges the range covered by one individual PSD function. The resulting master curve is comparable with the scattering data.

Results and discussion

After annealing for 8 h at 161 °C, which corresponds to a temperature within the unstable regime of the dPS/PpMS phase diagram, the samples exhibit dewetting structures at the surface [18]. A different type of dewetting structure was observed after storing the as-

prepared samples for 7 h in a toluene-vapor atmosphere. The sample surfaces as measured by AFM are shown in Fig. 2a, b. Due to the small polymer film thickness the resulting in-plane structures are small. Dewetting under a toluene-vapor atmosphere yields droplets of uniform height and similar but nonmonodisperse diameter (Fig. 2a), whereas the installed morphology after annealing appears more irregular (Fig. 2b). AFM pictures of the homopolymer samples look very similar. Consequently the observed surface morphology results from a dewetting process and not from a phase-separation process [39]. The observed structures differ significantly from the common droplet configurations resembling Voronoi tessellation patterns as observed for thicker films [2] in the case of dry dewetting and are reminiscent of the recently reported structures caused by wet dewetting [40]. In shape they agree well with morphologies observed with ultrathin films [10, 26]. While the dewetting of an initially homogeneous film commonly results from annealing above the glass-transition temperature, in a solvent-driven glass transition the polymer film is plasticized by incorporation of solvent molecules [41]. The original homogeneous polymer film is replaced by a highly concentrated polymer–toluene solution layer. Thus the surface tension, viscosity and van der Waals interaction with the substrate are markedly changed compared to the polymer melt. A detailed study of the dewetting is beyond the scope of this short communication and is given elsewhere [39].

From the AFM topography pictures presented in Fig. 2 no information about the internal distribution of the blend components can be obtained. Because both blend components (dPS and PpMS) differ only by one methyl group, despite deuteration, their chemical and mechanical properties are very similar; therefore, surface characterization methods such as friction and stiffness

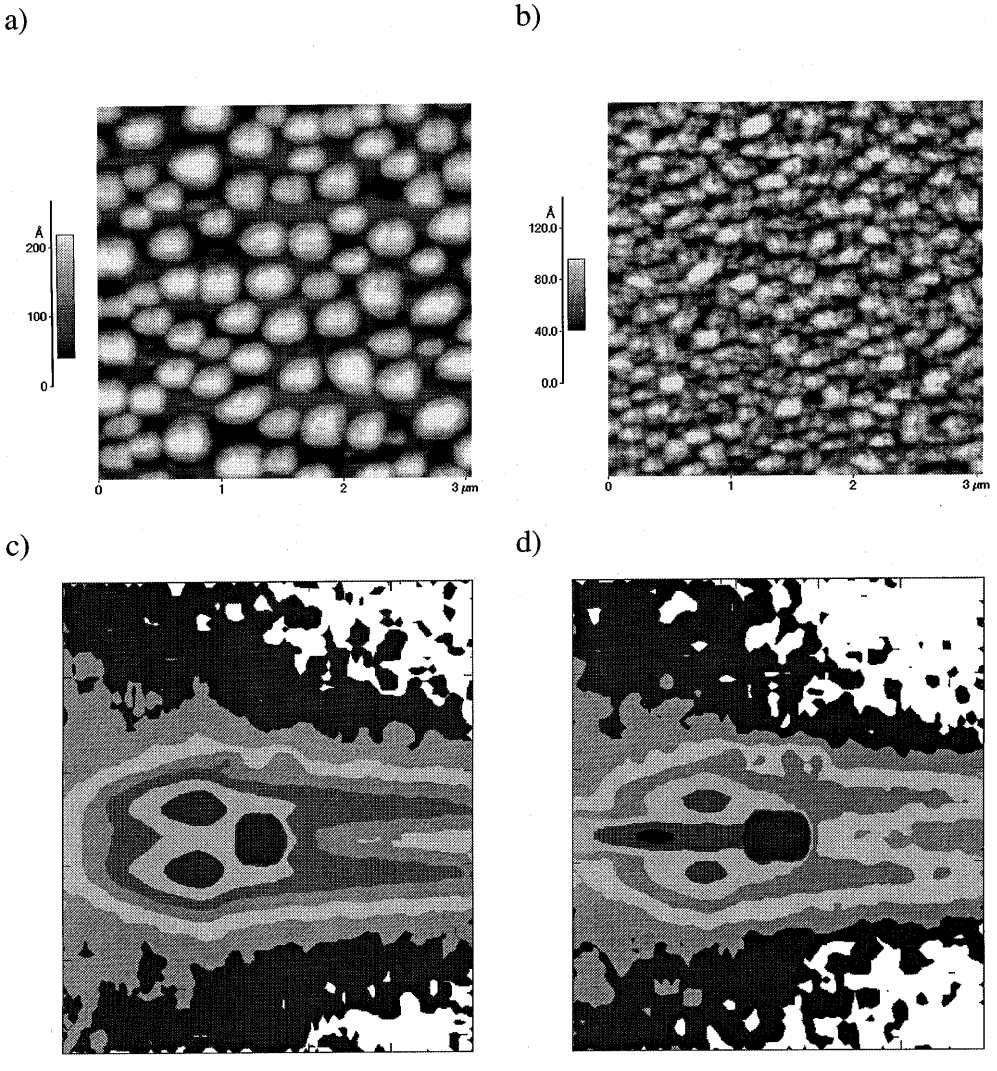

Fig. 2 a, b Atomic force microscopy (*AFM*) pictures (scan range $3 \times 3\mu m^2$) exhibiting the topology of the dewetted, confined poly(*p*-methyl styrene) (*PpMS*):deuterated polystyrene (*dPS*) blend films. In **a** the late stage the topography resulting from toluene-vapor treatment consists of isolated droplets whereas **b** after annealing the surface appears more irregular. AFM pictures of the homopolymer samples look similar. With GISANS differences between homopolymer and polymer blend samples are detected. Data from the samples dewetted under a toluene atmosphere are shown. The contour plots (**c**, **d**) have a logarithmic contour line spacing with an alternating color scheme. The left axis corresponds to the q_y direction and the bottom axis to the q_z direction. The specularly reflected peak is placed at the center of both contour plots. In each contour plot to the left the Yoneda peak is visible. In case of the homopolymer sample (**c**) it is split into two Yoneda peaks, whereas in case of the blend sample (**d**) a splitting into three peaks is observed. Each splitting into an even number of peaks corresponds to resolvable prominent in-plane length scales of the sample, whereas the absence of splitting or the presence of a central peak originate from nonresolvable lengths. For data evaluation horizontal slices are taken

measurements [42] do not yield enough contrast to distinguish between the components, and a selective dissolution [43] of one component is not possible. However, due to the contrast generated by deuteration, possible superstructures or substructures are detectable with GISANS. Figure 2c, d shows examples of the two-dimensional intensity distributions recorded at D22 at an angle of incidence $\alpha_i > \alpha_c$ above the critical angle of the polymer film and of the silicon substrate. In the case of rotational isotropic samples the scattering data is symmetric with respect to the $q_y = 0$ position (horizontal center of Fig. 2c, d). We used an alternating color scheme with a logarithmical contour line spacing to emphasize typical scattering features. The characteristics of the scattered intensity are separated: specular peak (black peak in the center of each plot) and Yoneda peak (two or three black peaks on the left of each plot). Comparing the measured intensities of the homopolymer (Fig. 2c) and the blend samples (Fig. 2d) significant differences are visible in the two-dimensional graphs. The region around the Yoneda peak shows quite different intensity distributions related to different chemical compositions as discussed later. The two-dimensional intensity distribution consists of several vertical and horizontal slices. The terms horizontally and vertically are used here with reference to the sample surface. Vertical slices at a constant out-of plane angle ψ (Fig. 1) correspond to conventional detector scans and horizontal slices at a constant detector angle $\Phi = \alpha_i + \alpha_f$ correspond to the out-of plane scans [44]. The (xy)-plane denotes the sample surface and $\vec{q} = (q_x, q_y, q_z)$ is the scattering vector.

The range of detectable in-plane length scales depends on the individual experimental set-up of the GISAS experiment, such as sample–detector distance and collimation [26]. At optimized experimental conditions the resolution of the two-dimensional detector used determines the smallest resolvable q value and thus the largest detectable in-plane length scale. An increase in the wavelength yields a further increase in this large length scale limit. On the other hand, this includes an increase in the small length scale limit which is basically given by the detector size. Of course a wavelength change is only performable within the limits of the individual instrument used and is frequently accompanied by a dramatic decrease in the primary intensity. The influence of a wavelength change on the resolution limit and on the corresponding detection of a most prominent in-plane length scale is demonstrated in Fig. 3. Using a plot with a double logarithmic axis the GISANS data from the confined homopolymer dPS film, which was dewetted under a toluene atmosphere, is shown as a function of the in-plane wave vector q_y. The GISANS experiment was performed at wavelengths of 0.7 nm, 1.0 nm and 1.4 nm. The different intensities mainly result from the changes in the incident flux after changing the wavelength. Each out-of plane scan shown was measured at one fixed q_z position, which corresponds to an exit angle, α_f, which is smaller than the critical angles of Si and dPS. Thus we are extremely sensitive towards the surface morphologies created by the dewetting structures. In the case of one most prominent in-plane length scale, ξ, the out-of-plane scan exhibits a peak at the corresponding position $q_{peak} = 2\pi/\xi$. As can be seen in Fig. 3 the position of this maximum intensity shifts with increasing wavelength towards smaller q_y values. This shift originated from an improvement in the experimental resolution. Thus the correct position of q_{peak} is only determinable at 1.4 nm without further data correction. If the measured peak appears near the resolution limit, the value of q_{peak} has to be determined by deconvolution of the data with the experimental resolution function.

Log-log plots of the intensity distribution of out-of plane scans measured at $q_z = 0.114\,\mathrm{nm}^{-1}$ are shown in Fig. 4. The cuts were performed at exit angles $\alpha_f = \alpha_c(\mathrm{PpMS}) < \alpha_c(\mathrm{Si})$, which also corresponds to exit angles below the critical angle of dPS. The intensity has been integrated in a vertical direction over a slice of $\Delta q_z = \pm 4.78 \times 10^{-3}\,\mathrm{nm}^{-1}$ to improve the statistics. Because the Fresnel transmission functions act in this geometry only as overall scaling factors, the intensity is given by the PSD function of an "effective surface" [43]. For comparison the master curve obtained from the AFM data is shown. Due to the same surface topography of dPS and of the blend sample as measured by AFM the master curves of both are the same and only one is shown.

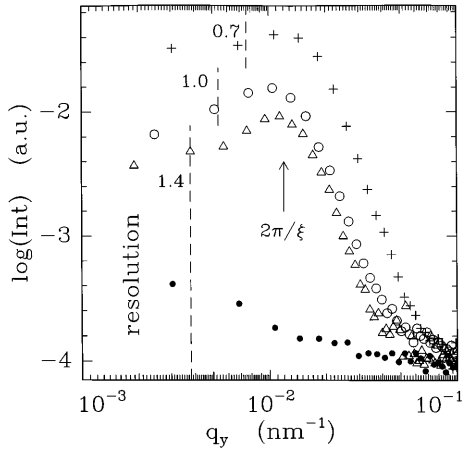

Fig. 3 Influence of the wavelength used on the resolution of the most prominent in-plane length scale. Horizontal slices from the 2D intensity distribution of the dewetted dPS sample are plotted on a double logarithmic axis. Measurements at wavelengths 0.7 nm (*crosses*), 1.0 nm (*circles*) and 1.4 nm (*triangles*) are compared. The resolution limit is shown by a *dashed line* (given number corresponds to the wavelength used). In addition the low background resulting from the empty sample holder (*dots*) is shown

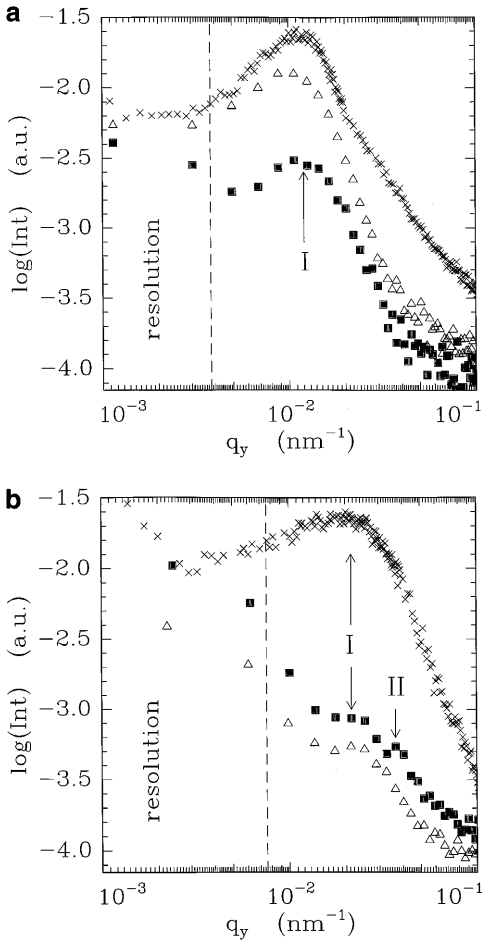

Fig. 4 a Comparison of the GISANS data from dPS (*triangles*) and PpMS:dPS (*filled squares*) samples dewetted after storage under toluene vapor. Within the resolvable length scale range one most prominent in-plane length, ξ, is detected at the marked position. The master curve from the AFM data (*crosses*) exhibits this in-plane length as well. The *dashed line* indicates the resolution limit. All curves are shifted for clarity. **b** Comparison of the GISANS data from dPS (*triangles*) and PpMS:dPS (*filled squares*) samples dewetted after annealing above the glass-transition temperature. Within the resolvable length scale range two dominant in-plane length scales, ξ_I and ξ_{II}, are marked with *arrows*. The master curve from the AFM data (*crosses*) exhibits only one in-plane length, ξ_I. The *dashed line* indicates the resolution limit. All curves are shifted for clarity

The PSD function measured for the samples dewetted under a toluene-vapor atmosphere are shown in Fig. 4a. A wavelength of 1.4 nm was used to resolve the peak in the PSD function without influence due to the resolution limit. On comparing GISANS measurements from the dPS sample and AFM measurements both the PSD function and the master curve exhibit a quite similar shape which is dominated by a well-pronounced peak (marked by "I"). In the master curve on the right-hand side of the peak a shoulder is visible which is not present in the scattering data. It might be attributed to a smeared-out form factor contribution related to the droplet shape. From the absence of the shoulder in the scattering spectrum it can be concluded that AFM always measures local information. The well-pronounced peak results from the most prominent in-plane length scale, $\xi = 525 \pm 5$ nm, and is related to the mean distance of the droplets; thus, each droplet consists of several polymer molecules [15, 18]. The GISANS data from the blend sample show a peak at the same positions containing the topological information. Additionally the intensity increases towards smaller q_y values and we observe a second peak inside the resolution limit. This peak is not present in the data from the dPS sample or in the AFM data. It results from length scales which are larger than the resolution limit. Therefore in the dewetted confined blend film in-plane lengths longer than 3.3 μm are present, suggesting the existence of a superstructure. From the measured data no actual number for this large length scale can be given. Further measurements at even longer wavelengths will be required to resolve the actual value.

Data taken from samples dewetted by annealing are compared in Fig. 4b. Both measurements, dPS and PpMS:dPS, exhibit one peak at a q_y position corresponding to an in-plane length scale of $\xi_I = (293 \pm 5)$ nm (marked "I"). Additionally the PpMS:dPS sample shows a second peak resulting from a smaller length scale of $\xi_{II} = (171 \pm 2)$ nm (marked "II") which appears to have a smaller full width at half-maximum due to the logarithmic x-axis. The intensity of the second peak is weak compared to the peak originating from ξ_I, but is well above the noise level. The symbol size gives an impression of the uncertainty of the data in the y-range of the second peak. It should be noted that in the master curve from the AFM data this peak at ξ_{II} is invisible, whereas the peak at ξ_I is even more pronounced; thus ξ_I corresponds to a topographical and ξ_{II} to a composition length scale. To detect this substructure with increased statistics both scans were measured at 0.7 nm which enlarges the resolvable length scale regime towards smaller in-plane lengths. Due to the more irregular surface topography (cf Fig. 2a, b) the peak in the PSD function from GISANS compared to that in the master curve from AFM is not that well pronounced. The larger length scales were not measured by AFM due to the small scan range compared to the coherently illuminated surface area in GISANS. In the scattering data they yield an increase in intensity towards smaller q_y values. The composition substructure observed suggests an internal structure with regular distances. In a thick-film system the minimization of the surface free energy yields segregation of the polymer with the lower surface tension at the surface. In a two-dimensional system the surface is replaced by the contact line and segregation at the contact line reduces the free energy. Additionally, the isolation of polymer

chains in a perpendicular direction forces a local phase-separation process [45]. Due to the strong confinement the system investigated can be regarded as two-dimensional. Each irregularly shaped droplet consists of several dPS and PpMS molecules which internally arrange to interact differently with the substrate. PpMS has a smaller surface tension compared to dPS [46]. After annealing in PpMS:dPS blend films with film thicknesses well above R_g, segregation of PpMS at the surface was observed [18]. Thus it seems reasonable that phase separation during annealing yields segregation of PpMS at the contact line of the individual droplets. This regular structure gives rise to the observed composition length scale at ξ_{II}. Additionally, during toluene-vapor treatment the interaction with the interpenetrated toluene molecules has to be taken into account. This might be the origin of the absence of a well-defined internal composition of the droplets.

Summary

In the case of confined homopolymer as well as polymer blend films the surface topography of the dewetted samples exhibits one most prominent in-plane length scale which corresponds to the mean distance of the droplets. AFM and GISANS are both able to resolve this in-plane length, which can therefore be regarded as representative for the whole sample. The droplets created by annealing are more irregular in their contact line compared to the ones which result from toluene-vapor treatment. The polymer blend samples additionally have composition inhomogeneities due to a phase-separation process; this cannot be detected by AFM. A smaller substructure in the case of the annealed samples and a larger super structure in case of the toluene-vapor-treated samples is detected with GISANS. Thus, in confined blend films of PpMS:dPS there is some trend to phase separation although the dewetting itself is not driven by the polymer incompatibility. GISANS combines the typical advantages of neutron experiments with advanced scattering techniques commonly used with X-rays. It is well suited to probe the roughness spectrum from a molecular to a mesoscopic in-plane length scale by tuning the wavelength used. Additionally, it provides information about the internal composition of the samples examined. On the other hand, GISANS experiments can only be performed at a limited number of experimental facilities since a high intensity and an excellent collimation are needed.

Acknowledgments This work was supported by the DFG Schwerpunktprogramm "Benetzung und Strukturbildung an Grenzflächen" (Sta 324/8-1). J.S.G. acknowledges support by the GKSS project V6.1.01.G.01-HS3.

References

1. Redon C, Brochard-Wyart F, Rondelez F (1991) Phys Rev Lett 66:715
2. Reiter G (1992) Phys Rev Lett 68:75
3. Reiter G (1993) Langmuir 9:1344
4. Liu Y, Rafailovich MH, Sokolov J, Schwarz SA, Zhong X, Eisenberg A, Kramer EJ, Sauer BB, Satija S (1994) Phys Rev Lett 73:440
5. Redon C, Brzoska JB, Brochard-Wyart F (1994) Macromolecules 27:468
6. Reiter G, Auroy P, Auvray L (1996) Macromolecules 29:2150
7. Jacobs K, Herminghaus S, Mecke KR (1998) Langmuir 14:965
8. Jacobs K, Seemann R, Schatz G, Herminghaus S (1998) Langmuir 14:4961
9. Kerle T, Yerushalim-Rozen R, Klein J (1998) Macromolecules 31:422
10. Xie R, Karim A, Douglas JF, Han CC, Weiss RA (1998) Phys Rev Lett 81:1251
11. Bruder F, Brenn R (1992) Phys Rev Lett 69:624
12. Steiner U, Klein J, Fetters L (1994) Phys Rev Lett 72:1498
13. Krausch G (1995) Mater Sci Eng R14:1–94
14. Sung L, Karim A, Douglas JF, Han CC (1996) Phys Rev Lett 76:4368
15. Tanaka K, Takahara A, Kajiyama T (1996) Macromolecules 29:3232
16. Karim A, Slawecki TM, Kumar SK, Douglas JF, Satija SK, Han CC, Russell TP, Liu Y, Overney R, Sokolov J, Rafailovich MH (1998) Macromolecules 31:857
17. Affrossman S, O'Neill SA, Stamm M (1998) Macromolecules 31:6280
18. Müller-Buschbaum P, O'Neill SA, Affrossman S, Stamm M (1998) Macromolecules 31:5003
19. Müller-Buschbaum P, Gutmann JS, Stamm M (1999) J Macromol Sci Phys B38:577
20. Krausch G (1994) Ber Bunsenges Phys Chem 98:446
21. Sanchez IC (1992) Physics of polymer surfaces and interfaces. Butterworth, London
22. Bilder K (1992) Annu Rev Chem 43:33
23. Reiter G (1993) Europhys Lett 23:579
24. Keddie JL, Jones RAL, Cory RA (1994) Europhys Lett 27:59
25. Gießler KH, Rauch F, Stamm M (1994) Europhys Lett 27:605
26. Müller-Buschbaum P, Vanhoorne P, Scheumann V, Stamm M (1997) Europhys Lett 40:655
27. Müller-Buschbaum P, Casagrande M, Gutmann J, Kuhlmann T, Stamm M, von Krosigk G, Lode U, Cunis S, Gehrke R (1998) Europhys Lett 42:517
28. Felcher GP, Russell TP (1991) Physica B 173:1
29. Russell TP (1990) Mater Sci Rep 5:171
30. Stamm M, Schubert DW (1995) Annu Rev Mater Sci 25:325
31. Sinha SK, Sirota EB, Garoff S, Stanley HB (1988) Phys Rev B 38:2297
32. Press W, Tolan M, Stettner J, Nitz V, Schlomka JP, Seeck OH, Müller-Buschbaum P (1996) Physica B 221:1
33. Salditt T, Metzger TH, Brandt Ch, Klemradt U, Peisl J (1995) Phys Rev B 51:5617
34. Pynn R (1995) Mater Res Soc Symp Proc 376:165
35. Felcher GP, Goyette RJ, Anastasiadis S, Russell TP, Foster M, Bates F (1994) Phys Rev B 50:9565
36. Li ZX, Lu JR, Thomas RK, Penfold J (1996) Faraday Discuss 104:127

37. Büttner HG, Lelievre-Berna E, Pinet F (1997) Guide to neutron research facilities at the ILL. Institut Laue-Langevin, Grenoble, p 32
38. Gutmann JS, Müller-Buschbaum P, Stamm M (1999) Faraday Discuss Vol 112
39. Müller-Buschbaum P, Gutmann JS, Stamm M (1999) Phys Chem Chem Phys (in press)
40. Fondecave R, Brochard-Wyart F (1999) Macromolecules 31:9305
41. Laschitsch A, Bouchard C, Habicht J, Schimmel M, Rühe J, Johannsmann D (1999) Macromolecules 32:1244
42. Krausch G, Hipp M, Böltau M, Mlynek J (1995) Macromolecules 28:260
43. Walheim S, Böltau M, Mlynek J, Krausch G, Steiner U (1997) Macromolecules 30:4995
44. Salditt T, Metzger TH, Peisl J, Goerigk G (1995) J Phys D Appl Phys 28:A236
45. de Gennes PG (1979) Scaling concepts in polymer physics. Cornell University Press, Ithaca
46. Schnell R (1997) PhD thesis. University of Mainz